2013

Morphology-controllable 1D-3D nanostructured TiO2 bilayer photoanodes for dye-sensitized solar cells

Ziqi Sun
University of Wollongong, ziqi@uow.edu.au

Jung Ho Kim
University of Wollongong, jhk@uow.edu.au

Yue Zhao
University of Wollongong, yue@uow.edu.au

Darren Attard
University of Wollongong, darrena@uow.edu.au

S X. Dou
University of Wollongong, shi@uow.edu.au

Morphology-controllable 1D-3D nanostructured TiO2 bilayer photoanodes for dye-sensitized solar cells

Abstract

Morphology-controlled bilayer TiO_2 nanostructures consisting of one-dimensional (1D) nanowire bottom arrays and a three-dimensional (3D) dendritic microsphere top layer were synthesized via a one-step hydrothermal method. These novel 1D-3D bilayer photoanodes demonstrated the highest energy conversion efficiency of 7.2% for rutile TiO_2 dye-sensitized solar cells to date, with $TiCl_4$ post-treatment.

Keywords

1d, 3d, nanostructured, tio2, bilayer, photoanodes, dye, sensitized, solar, cells, morphology, controllable

Disciplines

Engineering | Physical Sciences and Mathematics

Publication Details

Sun, Z., Kim, J., Zhao, Y., Attard, D. J. & Dou, S. Xue. (2013). Morphology-controllable 1D-3D nanostructured TiO2 bilayer photoanodes for dye-sensitized solar cells. Chemical Communications, 49 (10), 966-968.

ChemComm

Dynamic Article Links ►

Cite this: DOI: 10.1039/c0xx00000x

www.rsc.org/xxxxxx

COMMUNICATION

Morphology-controllable 1D/3D Nanostructured TiO_2 Bilayer Photoanodes for Dye-sensitized Solar Cells

Ziqi Sun [a], Jung Ho Kim [a,*], Yue Zhao [a], Darren Attard [b] and Shi Xue Dou [a]

Received (in XXX, XXX) Xth XXXXXXXXX 20XX, Accepted Xth XXXXXXXXX 20XX

DOI: 10.1039/b000000x

Morphology-controlled bilayer TiO_2 nanostructures consisting of one-dimensional (1D) nanowire bottom arrays and three-dimensional (3D) dendritic microsphere top layer were synthesized via one-step hydrothermal method. These novel 1D/3D bilayer photoanodes demonstrated the highest energy conversion efficiency of 7.2% for rutile TiO_2 dye-sensitized solar cells to date, with $TiCl_4$ post-treatment.

Innovations in materials technology in the fields of photovoltaic cells and photocatalysis are playing a key role in the paradigm shift from fossil fuels to renewable sources. Economically viable and stable energy conversion devices with efficiencies surpassing those presently available are fundamental to such a transition, requiring a new generation of materials that offer broad-spectrum light harvesting and superior charge transport properties.[1] Dye-sensitized solar cells (DSCs) have been recognized as one of the most promising devices for low-cost solar-to-electricity energy conversion. The improvement in DSC performance, however, has been impeded by the disordered structure of the mesoporous TiO_2 films in current DSCs, which induce a short electron diffusion length (10-35 μm) by interfacial dissipating, trapping and detrapping.[2] Usually, two ways to increase solar energy harvesting/conversion efficiency are employed by enhancing electron diffusion length and light harvesting in DSCs. The one is the application of vertically aligned one-dimensional (1D) nanostructures, which has been identified as a promising way to enhance the electron diffusion length (up to ~100 μm).[1, 3] One key challenge in using vertically aligned 1D nanostructures in DSCs is that they have a low internal surface area, resulting in insufficient dye adsorption, and therefore, low light-harvesting efficiency. The other way is adopting large nanostructures in sizes of ~400-800 nm to enhance the light scattering.[4] Unfortunately, the large particle size of the nanoparticles significantly lowers the surface area and the amount of dye uptake. In general, high specific surface area, long electron diffusion length, and a pronounced light-scattering effect are indispensable to a high-performance photoanode, but these factors are often incompatible with one another.

To accommodate all of these favourable characteristics, we propose an innovative one-step approach to synthesize double-layered structures with controlled morphology to act as DSC photoanode. In our design of the bilayer TiO_2 nanostructures, the bottom layer is vertically aligned 1D TiO_2 nanowires, which feature high photoinjected electron collection efficiency, fast electron transport, and a long electron diffusion length; while the top layer consists of three-dimensional (3D) TiO_2 dendritic nanostructures 1-3 μm in diameter and with high specific surface area that function simultaneously as an effective dye adsorptive and light-scattering layer.

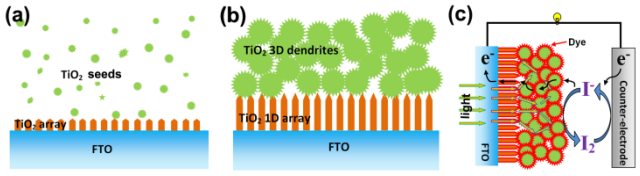

Scheme 1: Schematic diagram of the "one-step" synthesis of 1D/3D TiO_2 bilayer nanostructure for dye-sensitized solar cells application: (a) formation of TiO_2 nucleation seeds in solution and the surface of FTO glass; (b) growth and assembly of 1D nanowire arrays and 3D microspheres bilayer nanostructure; (c) the application of the 1D/3D TiO_2 bilayer nanostructure as photoanode of DSCs.

Scheme 1 presents the one-step synthesis of 1D/3D bilayer TiO_2 nanostructure on FTO substrate. In this process, the sedimentation of 3D TiO_2 dendrites by gravity was intelligently employed. First, the solution used for hydrothermal synthesis, a mixture of an aqueous Ti-containing precursor solution based on titanium tetraisopropoxide (TTIP) and cetyltrimethyl ammonium bromide (CTAB), with a molar ratio of $100H_2O$:7HCl:0.5CTAB: 0.1TTIP ($TTIP_{aq}$), together with ethylene glycol (EG) in different volume ratios ($TTIP_{aq}$:EG = 1:1, 1:4, 1:6), was put into a Teflon lined autoclave. Then, a FTO glass substrate was set on the bottom of the Teflon liner with the conducting layer facing up. In the initial hydrothermal stage, TiO_2 nanocrystalline centres (or seeds) began to form on the FTO surface and in the solution (Scheme 1(a)). At this time, the isolated crystals in solution are tiny enough for good dispersion. With the continuing synthesis reaction, oriented 1D TiO_2 nanostructure arrays on the FTO substrate form in the shape of nanowires as the bottom layer, and the 3D TiO_2 dendritic nanostructures form a sediment on the surface of the array as the top layer (Scheme 1(b)). The morphology of the oriented 1D arrays or the 3D nanodendrites, or the size of the 3D dendritic particles can be controlled by adjusting the volume ratio of EG to $TTIP_{aq}$. The finished nanostructured photoanodes can be finally obtained after heating and then assembled into DSCs (Scheme 1(c)). The details of the experimental procedures can be found in the Supporting Information.

The morphology and microstructure of the bifunctional TiO_2 photoanodes synthesized from the solution with a volume ratio of

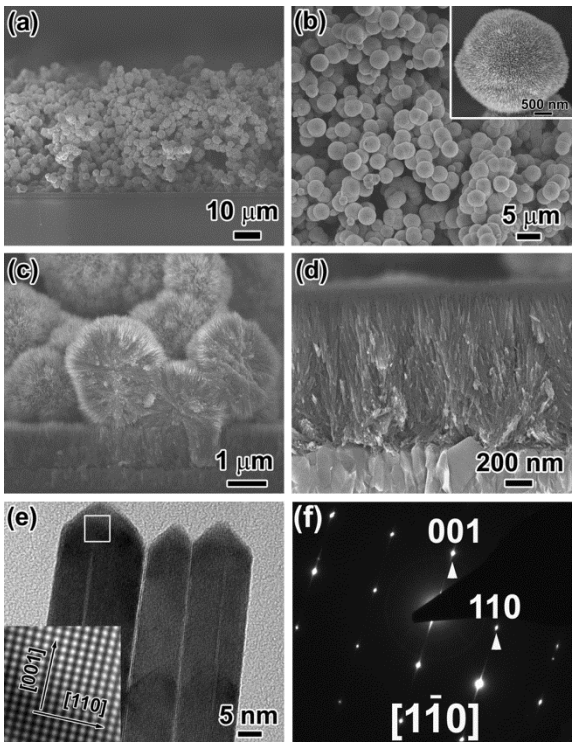

Figure 1: Morphologies of the bilayer TiO_2 nanostructures synthesized from the solution with a composition of $TTIP_{aq}$:EG = 1:1: (a) low magnification cross-sectional SEM image of the synthesized bilayer structure; (b) SEM top-view of the bilayer structure surface, where the inset is a high magnification SEM image of the 3D dendritic TiO_2 nanostructures; (c) high magnification SEM image of the interface between the 1D nanowire array and the 3D dendritic top-layer; (d) high magnification SEM image of the underlayer showing the 1D nanowire array; (e) HRTEM characterization of the nanowires in the 1D arrays and the 3D dendrites, with the inset showing an enlargement of the area in the white square; and (f) the corresponding SAED pattern to (e).

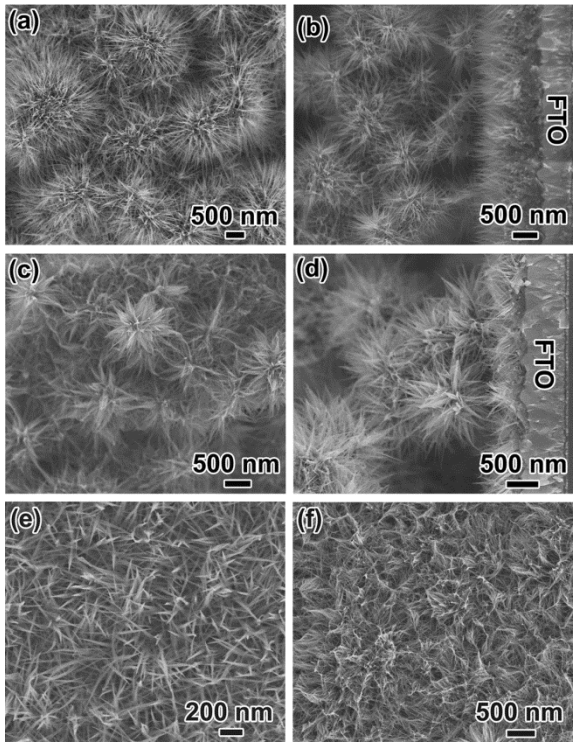

Figure 2: SEM top-views (left) and the cross-sectional views (right) of the bilayer nanostructures synthesized in solution with compositions of (a-b) $TTIP_{aq}$:EG = 1:4 and (c-d) $TTIP_{aq}$:EG = 1:6; (e-f) SEM images of the nanowires in the 1D nanowire array underlayer of the bilayer nanostructure after removal of the top 3D dendrites, with synthesis from solutions containing (e) $TTIP_{aq}$:EG = 1:4 and (f) $TTIP_{aq}$:EG = 1:6.

$TTIP_{aq}$:EG = 1:1 were examined by SEM and TEM, as shown in Figure 1. Fig. 1(a) shows a cross-sectional SEM image of the bifunctional photoanode. It reveals that a continuous 3D TiO_2 dendrite network has formed as the top layer with a thickness of ~40 μm, and the particle size of the TiO_2 microspheres is in the range of 2-3 μm (Fig. 1(b)). It is very interesting that the TiO_2 microspheres are not dense solid balls, but 3D dendritic nanostructures made up of nanowires approximately 10 nm in diameter as nano-units (inset in Fig. 1(b)). This 3D dendritic TiO_2 nanostructure has been proved to possess high specific surface area and superior electrochemical properties compared to nanoparticles with smooth surfaces.[5] The bottom nanowire arrays had a similar shape and dimensions to those of the constituent units of the 3D dendrites. The thickness of the TiO_2 nanowire arrays was around 1.5 μm (Fig. 1(c-d)). As shown in Fig. 1(c), a strong mechanical connection between the microspheres or between the microspheres and the nanowire arrays was observed on a fractured surface. The growth directions and microstructures of the constituent nanowires of the 1D nanostructure arrays and the 3D dendrites were examined by HRTEM (Fig. 1(e-f)). The nanowires are well-crystallized in rutile TiO_2 single-crystals, where the growth direction is along the [001] orientation and the side surfaces are {110} facets. The single-crystal characteristics of the nanowires are very crucial in DSC application, as they will provide fast electronic transport through the wires, and most importantly, avoid the surface defect trapping derived by poor crystallization. The XRD patterns show that the obtained TiO_2 nanostructures were well-crystallized as rutile phase (Fig. S1).

By adjusting the $TTIP_{aq}$/EG volume ratio, the 1D/3D bilayer nanostructures with different constituent nanowire diameters were synthesized. The diameter of the nanowires synthesized from the mixed solution with a volume ratio of $TTIP_{aq}$:EG = 1:1 was around 10 nm, as can be seen in Fig. 1 (denoted as NW-C), then changed to ~6 nm when $TTIP_{aq}$:EG = 1:4, and to ~4 nm with $TTIP_{aq}$:EG = 1:6 (denoted as NW-F, Fig. 2). Due to the dilution of Ti-containing precursor by EG in the reaction solutions, both the thicknesses of the nanowire arrays and the overall size of 3D dendrites were decreased as the increasing of EG contents. By repeating the deposition 2-5 times, the thickness of the dendritic microsphere scattering layer can be increased to 40 μm. This repeated treatment, however, has no effect on increasing the thickness of the bottom nanowire array. Owing to the thinness of the bilayer nanostructures synthesized from the solution with $TTIP_{aq}$:EG = 1:6, we picked the bilayer thin films obtained from the solutions of $TTIP_{aq}$:EG = 1:1 (NW-C) and $TTIP_{aq}$:EG = 1:4 (NW-F) for further photochemical characterizations.

In the UV-Vis spectra (Fig. S2), the cut-off edge of the nanowire single-layer thin film spectrum is around 390 nm, corresponding to a band-gap of 3.2 eV, which is much wider than the band-gap of bulk rutile TiO_2 (3.0 eV), attributing to the quantum size effect of the small nanowires.[17] However, two conspicuous peaks were detected in the absorbance spectrum of the 1D/3D bilayer structure. The first peak located at 350 nm

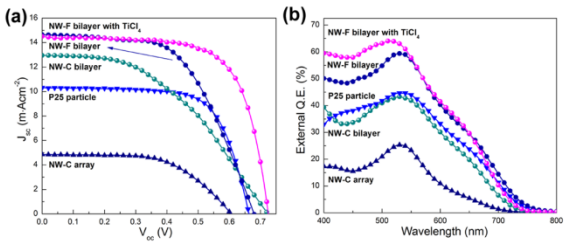

Figure 3: (a) J-V curves and (b) IPCE active spectra of the DSCs with different pohotoanodes.

should be assigned to the absorption of the constituent nanowires. The second absorption at ~400 nm (3.1 eV) was contributed by the large-size cores of the 3D dendritic microspheres. The most interesting phenomenon in the UV-Vis absorption spectra is that there is a strong scattering effect from the bilayer thin films in visible light regime, which is helpful for confining and harvesting the incident light within the electrode.

Fig. 3 shows typical photocurrent density - photovoltage (*J-V*) curves (Fig. 3(a)) and the external quantum efficiencies in the 400-800 nm wavelength range (Fig. 3(b)) of the solar cells made from photoanodes with the following configurations: single-layer 1D TiO_2 nanowire arrays (NW-C arrays, ~1 μm in thickness), single-layer commercial P25 nanoparticles (~10 μm in thickness), and bifunctional TiO_2 nanostructures (NW-C bilayers and NW-F bilayers, ~1.0 μm 1D TiO_2 nanowire array underlayer plus ~19 μm 3D TiO_2 microsphere top layer). The measured results on these solar cells are summarized in Table 1.

The solar cells with NW-C array photoanode showed the lowest energy conversion efficiency, where the V_{oc} was 0.61 V, J_{sc} was 4.86 mA·cm^{-2}, *FF* was 0.58, and η was 1.7%. For the NW-C bilayer photoanodes, the energy conversion was significantly enhanced to 4.3%, corresponding to an enhancement of 150% over the NW-C single-layer photoanode. In the IPCE action spectrum of the NW-C bilayers, there is obvious visible light energy conversion in the wavelength range from 600-750 nm. The solar cell efficiency was further improved by employing NW-F bilayer photoanodes, which exhibited a V_{oc} of 0.68 V, J_{sc} of 14.70 mA·cm^{-2}, *FF* of 0.56, and η of 5.6%, better than the commercial P25 TiO_2 nanoparticle photoanode.

Even though improvements in V_{oc} and J_{sc} were observed in the 1D/3D bilayer photoanode, the *FF* showed a decrease from 0.69 for P25 photoanodes to 0.44 for the ones with NW-C bilayer photoanodes and 0.56 for the ones with NW-F bilayer photoanodes. This kind of *FF* decrease for the bilayer photoanodes is likely to be the high internal resistance in the 3D dendritic TiO_2 microsphere scattering layer. $TiCl_4$ soaking was used to overcome this disadvantage, as it can increase the contact among the 3D dendritic microspheres and thus decrease the internal resistance of the TiO_2 bilayer photoanodes (Fig. S3).[6] On comparing the solar cell performance of the NW-F bilayer photoanodes before and after $TiCl_4$ treatment, the *FF* improved significantly from 0.56 to 0.68, and contributed to a cell efficiency enhancement from 5.6% to 7.2%. The $TiCl_4$ post-treatments exhibited a significant enhancement on the DSC efficiency, due to the improved connection among the 1D and 3D nanostructures. The high efficiency of DSCs achieved by the bifunctional photoanodes demonstrates the success of our strategy of designing novel 1D/3D bilayer nanostructures that simultaneously combines previously incompatible factors for superior DSCs, such as high specific surface area, long electron diffusion length, and a pronounced light-scattering effect.

Table 1: Photovoltaic performance of the solar cells with different photoanodes.

Photoanodes	V_{oc} (V)	J_{sc} (mA·cm^{-2})	FF	η (%)
NW-C array	0.61	4.86	0.58	1.7
P25 particle	0.66	10.32	0.69	4.7
NW-C bilayer	0.74	12.95	0.44	4.3
NW-F bilayer	0.68	14.70	0.56	5.6
NW-F bilayer with $TiCl_4$	0.72	14.51	0.68	7.2

Conclusions

Novel morphology-controlled 1D/3D bilayer TiO_2 nanostructures were synthesized via a simple one-step hydrothermal method. These bilayer nanostructures simultaneously possess the incompatible features of high specific surface area, fast electron transport, and a pronounced light-scattering effect, and provide DSCs an energy conversion efficiency of 7.2% after $TiCl_4$ treatment, compared to 4.7% for the commercial P25 TiO_2 nanoparticle photoanode. The successful synthesis of these novel photoanodes opens up a new way to improve the performance of DSCs.

This work was supported by Australian Research Council Discovery Project DP1096546.

Notes and references

[a] *Institute for Superconducting and Electronic Materials, University of Wollongong, Innovation Campus, Squires Way, North Wollongong, NSW 2500, Australia, E-mail: jhk@uow.edu.au*
[b] *AIIM Electron Microscopy Centre, University of Wollongong, Innovation Campus, Squires Way, North Wollongong, NSW 2500, Australia*

† Electronic Supplementary Information (ESI) available: XRD patterns, UV-vis spectra, and SEM images. See DOI: 10.1039/b000000x/

1 (a) B O'Regan, M. Grätzel, *Nature*, 1991, **353**, 737; (b) A. Hagfeldt, G. Boschloo, L. Sun, L. Kloo, H. Pettersson, *Chem. Rev.*, 2010, **110**, 6595; (c) O. K.Varghese, M. Paulose, C. A. Grimes, *Nat. Nanotech.*, 2009, **4**, 592.

2 (a) J. Liao, B. Lei, D. Kuang and C. Su, *Energy Environ. Sci.*, 2011, **4**, 4079; (b) W. Wu, J. Liao, H. Chen, X. Yu, C. Su, D. Kuang, *J. Mater. Chem.* 2012, **22**, 18057.

3 (a) M. Wang, Y. Wang and J. Li, *Chem. Comm.*, 2010, **46**, 11246; (b) P. Roy, S. Berger and P. Schmuki, *Angew. Chem. Int. Ed.*, 2011, **50**, 2904; (c) J. Boucle, S. Chyla, M. Shaffer, J. Durrant, D. Bradley and J. Nelson, *Adv. Funct. Mater.*, 2008, **18**, 622; (d) L. Yang, W. W. Leung, *Adv. Mater.*, 2011, **23**, 4559; (e) J. R. Jennings, A. Ghicov, L. M. Peter, P. Schmuki and A. B. Walker, *J. Am. Chem. Soc.*, 2008, **130**, 13364; (f) M. Law, L. E. Greene, J. C. Johnson, R. Saykally, and P. Yang, *Nat. Mater.*, 2005, **4**, 455.

4 (a) W. Shao, F. Gu, L. Gai and C. Li, *Chem. Comm.*, 2011, **47**, 5046; (b) S. Ito, S. M. Zakeeruddin, R. Humphty-Baker, P. Liska, R. Charvet, *Adv. Mater.*, 2006, **18**, 1202; (c) H. Koo, Y. J. Kim, Y. H. Lee, W. I. Lee, K. Kim, and N. G. Park, *Adv. Mater.*, 2008, **20**, 195; (d) Z. Q. Sun, J. H. Kim, Y. Zhao, F. Bijarbooneh, V. Malgras, S. X. Dou, *J. Mater. Chem.*, 2012, **22**, 11711.

5 Z. Q. Sun, J. H. Kim, Y. Zhao, F. Bijarbooneh, V. Malgras, Y. Lee, Y. Kang, S. X. Dou, *J. Am. Chem. Soc.*, 2011, **133**, 19314.

6 (a) N. Satoh, T. Nakashima, K. Kamikura and K. Yamamoto, *Nat. Nanotech.*, 2008, **3**, 106; (b) N. Fuke, R. Katoh, A. Islam, M. Kasuya, A. Furube, A. Fukui, Y. Chiba, R. Komiya, R. Yamanaka, L. Han and H. Harima, *Energy Environ. Sci.*, 2009, **2**, 1205; (c) S. Ito, P. Liska, P. Comte, R. Charvet, P. Pechy, U. Bach, L. Schemidt-mende, S. Zakeeruddin, A. Kay, M. Nazeeruddin and M. Gratzel, *Chem. Comm.*, 2005, **34**, 4351.